RESEARCH ARTICLE

Material properties of skin in the flying snake *Chrysopelea ornata*

Sarah B. Dellinger[1] | Raffaella De Vita[2] | Pavlos P. Vlachos[3] | Martha M. Muñoz[4] | John J. Socha[2] ®

[1]Aerodyne Industries, Cape Canaveral, Florida, USA

[2]Department of Biomedical Engineering and Mechanics, Virginia Tech, Blacksburg, Virginia, USA

[3]School of Mechanical Engineering, Purdue University, West Lafayette, Indiana, USA

[4]Department of Ecology and Evolutionary Biology, Yale University, New Haven, Connecticut, USA

Correspondence
John J. Socha, Department of Biomedical Engineering and Mechanics, Virginia Tech, Blacksburg, VA 24061, USA.
Email: jjsocha@vt.edu

Abstract

In snakes, the skin serves for protection, camouflage, visual signaling, locomotion, and its ability to stretch facilitates large prey ingestion. The flying snakes of the genus *Chrysopelea* are capable of jumping and gliding through the air, requiring additional functional demands: its skin must accommodate stretch in multiple directions during gliding and, perhaps more importantly, during high-speed, direct-impact landing. Is the skin of flying snakes specialized for gliding? Here, we characterized the material properties of the skin of *Chrysopelea ornata* and compared them with two nongliding species of colubrid snakes, *Thamnophis sirtalis* and *Pantherophis guttatus*, as well as with previously published values. The skin was examined using uniaxial tensile testing to measure stresses, and digital image correlation methods to determine strains, yielding metrics of strength, elastic modulus, strain energy, and extensibility. To test for loading orientation effects, specimens were tested from three orientations relative to the snake's long axis: lateral, circumferential, and ventral. Specimens were taken from two regions of the body, pre- and pos-tpyloric, to test for regional effects related to the ingestion of large prey. In comparison with *T. sirtalis* and *P. guttatus*, *C. ornata* exhibited higher post-pyloric and lower pre-pyloric extensibility in circumferential specimens. However, overall there were few differences in skin material properties of *C. ornata* compared to other species, both within and across studies, suggesting that the skin of flying snakes is not specialized for gliding locomotion. Surprisingly, circumferential specimens demonstrated lower strength and extensibility in pre-pyloric skin, suggesting less regional specialization related to large prey.

KEYWORDS
elastic modulus, extensibility, flying snake, material properties, skin, strain energy, strength

1 | INTRODUCTION

The skin of snakes is a multifunctional organ. It acts to protect underlying structures from outside elements (Frolich, 1997), serves as camouflage from predators and prey (Osorio & Srinivasan, 1991), facilitates heat transfer (Frolich, 1997), and maintains a homeostatic hydration level (Licht & Bennett, 1972; Rivera et al., 2005). The skin may also function as a vasoconstrictor to prevent blood from pooling when the body is oriented vertically, particularly in tree snakes (Lillywhite, 1993). In macrostomates (snakes that ingest large prey, a clade encompassing most snake species), large food items can be accommodated because the skin stretches circumferentially, largely in the anterior body (Moon, 2000; Rivera et al., 2005), reaching extremes of multiple body-diameter increases in Dasypeltis, the egg-eating snakes (Gans, 1953). Extreme stretch has been quantified in watersnakes (Nerodia sipedon), with the skin of the lower jaw reaching a 10X length without failure (Close & Cundall, 2014). For all snakes, the skin represents the only site of contact between the body and the substrate and, correspondingly, it also plays a major role in locomotion. It must be stiff enough to transmit musculoskeletal forces for propulsion, but also compliant enough to accommodate other functions that require stretching. Across modes of locomotion in snakes, from slithering and climbing on solid substrates to swimming and gliding through fluids, the material properties of the skin must be able to accommodate trade-offs and meet the needs of multiple functions. In this study, we examine the properties of skin in relation to snakes that perform a unique mode of locomotion: gliding through the air (Socha, 2002).

Mechanically, snake skin can be considered a composite structure. The outermost portion is composed of an array of stiff scales, which are embedded in a less stiff, elastic layer. Only the central portion of each scale is directly attached to the underlying layers, with the outer edges of the scale overlapping others in the area known as the free margin. The percentage of scale overlap and integration to deeper layers varies among species (Jackson & Reno, 1975). The skin directly below the free margin is folded, and when loaded, begins to unfold rather than stretch, an important characteristic that plays a large role in the skin's multifunctional behavior (Savitzky et al., 2004). Compositionally, the skin is made mostly of collagen, elastin, and multiple types of keratin (Alibardi, 2005; Jackson & Reno, 1975), with relative concentrations of each varying across skin layers (Alibardi, 2005). At both the macro-and microscales, snake skin is nonhomogeneous (Figure 1), making mechanical testing and prediction of its behavior difficult, and requiring empirical studies to understand its properties.

Flying snakes (genus Chrysopelea) experience a range of mechanical demands on their skin. In addition to the typical functions encountered by macrostomates, their skin must accommodate the requirements of gliding, including takeoff (Socha, 2006), aerial undulation (Yeaton et al., 2020), and landing (Socha, 2011). When flying snakes glide, they typically launch into the air using a J-loop take-off, during which the posterior body grips the substrate and the anterior body moves upward with an acceleration of ~2 *g*

(Socha, 2006). Gripping forces during takeoff are mediated by both the ventral and lateral skin. During aerial undulation, the body moves with high-amplitude waves (with both horizontal and vertical components) at a frequency of 1–2 Hz; at the same time, the body cross-section maintains a flattened shape. Flattening manifests as the snake becomes airborne, with body width approximately doubling near the midsection and tapering toward the head and vent. This combination of undulation and dorsoventral flattening means that the skin is required to stretch in multiple directions, both circumferentially and longitudinally, and some combination therein (however, exact strains and strain rates are unknown). Lastly, because snakes have no limbs, flying snakes land by direct body collision with the receiving substrate. Flying snakes do not appear to slow down before landing, and impact speeds of 10 m/s or greater suggest that the skin and other anatomy must absorb large impact forces (estimated as large as ~20X body weight; Socha, 2011) and experience complex loading regimes. Even if strains are small, the short timescale of contact during landing (less than a second) means that skin could be experiencing high strain rates. It is not known how often (or why) snakes glide, but these events may represent maximum loading and potential for injury or death in the life history of the snake. Overall, the unique behaviors employed by flying snakes in gliding suggest that the skin may be specialized to accommodate the extremes required by this form of locomotion.

In this study, we characterize the mechanical behavior of the skin of one species of flying snake (the golden tree snake, Chrysopelea ornata). Using uniaxial tensile testing and digital image correlation (DIC), we loaded specimens to failure and determined the strength, stiffness, extensibility, and strain energy of the skin throughout the trunk, at multiple orientations. For comparison with non-gliding species, we additionally examined two other species that are not closely related to Chrysopelea, the common garter snake Thamnophis sirtalis and the corn snake Pantherophis guttatus. The genus Chrysopelea is one of four members of the subfamily Ahaetuliinae (Figueroa et al., 2016), a group of arboreal taxa from Southeast Asia that also includes Ahaetulla, Dendrelaphis, and Dryophiops. Thamnophis and Pantherophis are members of the subfamilies Natricinae and Colubrinae (Pyron et al., 2013), respectively. We also chose these comparison species because they are colubrids that have been used previously in studies that involve skin properties (Hu et al., 2009; Rivera et al., 2005). Furthermore, T. sirtalis is one of the few species to receive a detailed investigation of mechanical properties (Rivera et al., 2005), and therefore is particularly useful for comparison across studies that use different techniques. Using these three species, we address two hypotheses of skin properties in the context of gliding locomotion: (1) The skin of Chrysopelea should be stronger and/or have greater energy absorption capabilities, owing to the impact forces imparted upon landing. (2) The skin of Chrysopelea should be more regionally homogenous in material properties; the dorso-ventral flattening that stretches the skin occurs throughout the body, and any impact forces that are experienced can occur anywhere on the body. Implicit in this hypothesis is that the

FIGURE 1 Morphology of the skin of *Chrysopelea ornata*. (a) Dorsal, (b) ventral, and (c) lateral views of the snake's body, showing the configuration of scales from a specimen immediately after euthanasia. The anterior is to the top in (a, b), and to the left in (c). Scale bar = 10 mm. (d, e) A comparison of the lateral scales in the relaxed state (d) and manually stretched state (e); anterior is to the left. The stretched state in (e) shows the insertion locations of the scales, which are embedded in the underlying skin. The insertion is on the anterior and ventral margins of the scales; the dorsal and posterior edges are free, enabling the scales to overlap when at rest. Scale bar = 2 mm. The location and orientation of the skin specimens are shown in (f, g). The skin before specimen cutting is shown laid out in a flattened configuration in (f), with the ventral skin on the bottom and anterior to the left.
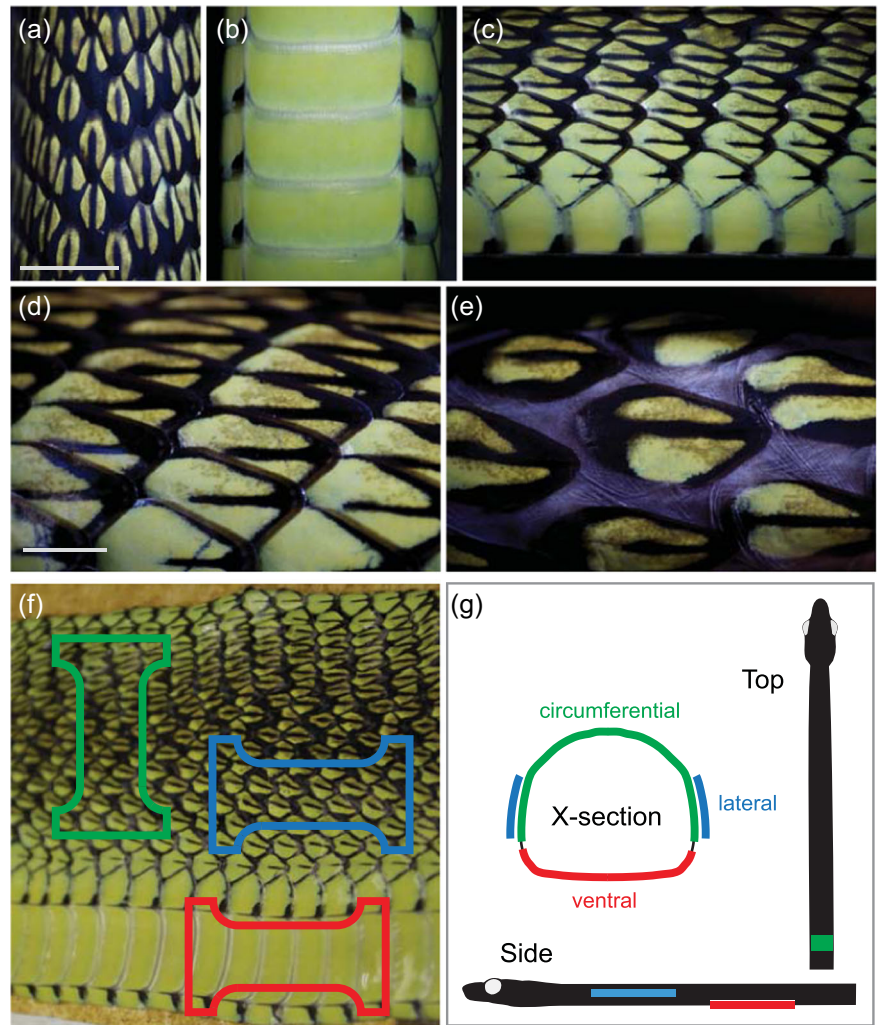
functional demands related to aerial locomotion are greater than those required for feeding on large prey items, which is thought to account for regional specializations in macrostomatan snakes (Rivera et al., 2005). Because this study does not address these hypotheses in a quantitative phylogenetic context, the results here should be viewed as a first step toward addressing the potential specialization of the skin of *Chrysopelea* to accommodate the functional demands of aerial locomotion.

2 | MATERIALS AND METHODS

We investigated the mechanical properties of skin in three species of colubrid snakes by performing uniaxial tensile testing on freshly excised skin specimens. A DIC technique was used to determine the spatially resolved strain throughout each test, enabling a comprehensive characterization of the strain response of the snake skin to tensile loading. All animal procedures were approved by the Virginia Tech Institutional Animal Care and Use Committee (IACUC #10-098-ESM) and the Army Research Office (ARO #57949-LS-DRP).

2.1 | Animals

Snakes were obtained from commercial dealers (Glades Herp Farm and Reptiles-N-Critters). The skin was tested from three flying snakes, specifically the golden tree snake (*C. ornata* Shaw), five red rat snakes (*P. guttatus* Linnaeus), and two garter snakes (*T. sirtalis* Linnaeus). Animals were housed in individual enclosures with a 12–12 h light cycle, fed a diet of dead mice or live lizards, and supplied with water *ad libitum*. Animals were selected for testing during the period when their skin is considered "normal" (*i.e.*, before the beginning of a shed cycle), and euthanized using an intracoelomic injection of pentobarbital sodium (350 mg/ml Fatal-Plus; Vortech Pharmaceutical) at a dosage of 1 ml/100 kg body mass. One snake (*C. ornata* 3; Supporting Information: Table 1) that otherwise appeared healthy died of unknown causes and was immediately frozen for later testing. Previous studies show conflicting effects of freezing on skin tissue properties. Several studies indicate that few or negligible effects occur after the tissue has been frozen (Chan & Titze, 2003; Foutz et al., 1992; Jackson et al., 1991; Jørgensen et al., 1989; Marangoni et al., 1966; Woo et al., 1986; Wu et al., 2007), whereas others have suggested that freezing has significant effects on tissue (Clavert et al., 2001; Quirinia & Viidik, 1991). During the time period of

experimentation, we had limited ability to obtain *C. ornata* (which originates in Southeast Asia), and so we chose to include this specimen.

2.2 | Specimen preparation

To begin the removal of the skin, the euthanized snake was first decapitated using a razor blade. The skin was then slit through the lateral edge of the ventral scales along the length of the body. The skin was pulled slightly to expose the connective tissue between the skin and underlying musculature. This connective tissue was also cut, separating the skin from the snake's body. The skin was spread onto a paper towel wetted with Ringer's solution and was kept moisturized during the remainder of specimen preparation. We used a Ringer's solution previously employed in a study of garter snakes (*T. sirtalis*) (Cinelli et al., 2002), with a composition of 119 mM NaCl, 4.1 mM KCl, 2.5 mM $CaCl_2$, 1.5 mM $MgCl_2$, 15 mM glucose, 5 mM sodium pyruvate, and 10 mM HEPES.

At each region of interest along the length of the body, three types of specimens were cut: two types of longitudinally oriented specimens, from ventral skin (hereafter, "ventral specimens") and lateral skin (hereafter, "lateral specimens"), and one type of circumferentially oriented specimen, from dorsal skin (hereafter, "circumferential specimens") (Table 1; Figure 1f,g;). Because potential differences may exist between anterior and posterior ends of the snake related to feeding specializations (Rivera et al., 2005), we additionally identified specimens as either pre- or post-pyloric, as determined from location by dissection (approximately 50%–70% SVL, depending on species). Dog-bone-shaped specimens with a gage section 10 mm long and 6–8 mm wide were cut from these areas using scissors; this shape served to minimize end effects by promoting stress concentration in the middle of the specimen. Specimen thickness was determined using digital images (Nikon D90; Nikon) from a microscope (Stemi 2000-C; Carl Zeiss) before testing. For this measurement, the specimen was loosely sandwiched between two flat pieces of plastic and held orthogonally to the optical axis. Three thicknesses from each specimen were measured and averaged from the center of the gage region, with pixel distances determined using graphic design software (Microsoft Paint). Pieces of sandpaper (100 grit, ~15 × 5 mm^2) were then glued to the ends of the specimens using cyanoacrylate adhesive to enable gripping and avoid slippage. These sandpaper pieces were glued to strips of thin plastic for easier insertion of the specimens into the grips of the tensile testing machine (described below) and to prevent unnecessary stretching of the specimen during the remainder of preparation. Specimens were then stored at ~2°C in a sealed container humidified with Ringer's solution to maintain hydration until testing.

Before testing, specimens were speckle-coated with black acrylic paint using an airbrush (Badger 150; Badger Air-Brush Co.). This speckle-coating provided high-contrast markers for DIC (Zhang et al., 2005) during postprocessing analyses. After allowing the paint to dry for approximately 30 s, the specimens were rehydrated and chilled at 2°C until testing.

2.3 | Experimental setup

Tensile tests to failure were conducted using a commercial tensile tester (ElectroPuls E1000; Instron) with a 250 N load cell (Dynacell; Instron). In each trial, the specimen was first mounted in custom-made mechanical grips and hand-tightened. The specimens were submerged fully in a bath of Ringer's solution for the duration of testing (Figure 2e). Testing was conducted at room temperature (21–23°C). Specimens were preconditioned using a sine-wave extension pattern with an amplitude of 0.5 mm and frequency of 1 Hz for 10 cycles. Following preconditioning, specimens were held at 1 mm extension for 15 s, and then returned to the initial position, which was then defined as the zero-extension position. The specimens were allowed to rest for 5 min to reduce the potential viscoelastic effects of preconditioning. The specimens were then extended to failure at a constant extension rate of 0.9 mm·s^{-1}, based on an estimation of extension rate from the frequency and amplitude of aerial undulation, ~1–2 Hz and ~0.1 m, respectively (Socha et al., 2010). The true extension rate of the skin during gliding is not known, and the value we used should be considered only a rough estimate. During each trial, video of both surfaces (interior and exterior) of the skin was recorded simultaneously using two high-speed cameras (APX-RS; Photron). The inner surface of the specimen (Figure 2ai,b–d) was viewed by one camera directly, while the exterior surface of the specimen (Figure 2aii) was viewed with a second camera using a mirror positioned behind the specimen (Figure 2e,f). Recordings of each surface enabled us to evaluate the potential effects of the scales on strain patterns. Bluehill 2 software (Instron) and FASTCAM Viewer (PFV; Photron) software were used to record the force and video data, respectively, at a sampling rate of 50 Hz and 250 frames/s, respectively. Force data and image collection were synchronized using a trigger signal controlled by the Bluehill 2 software. The width of the specimen was determined from the first frame of the video recordings, measured midway along the length at its narrowest location.

A total of 285 specimens were tested, from which 180 were deemed suitable for analysis. Trials in which the specimens failed at the grips, slipped from the grips, or had unusable images due to overexposure were excluded. All tests were conducted within 72 h of euthanasia (or thawing in the case of the single frozen specimen), with most tests occurring within 48 h. This duration was determined as reasonable from preliminary tensile tests of circumferential specimens harvested from the skin of a *P. guttatus* snake at 6.5, 20, 31, 48, 72, and 100 h after euthanasia (Supporting Information: Figure S1).

2.4 | Data collection and analysis

The DIC method was used to determine the displacement field of each specimen throughout a test along the loading direction. Specifically, we used a custom particle image correlation analysis program (Prana, available at https://github.com/aether-lab/prana/; Eckstein & Vlachos, 2009) to perform the DIC. We chose to use this program, which is typically used to analyze grayscale particle image velocimetry images, because it was well suited to analyze the images
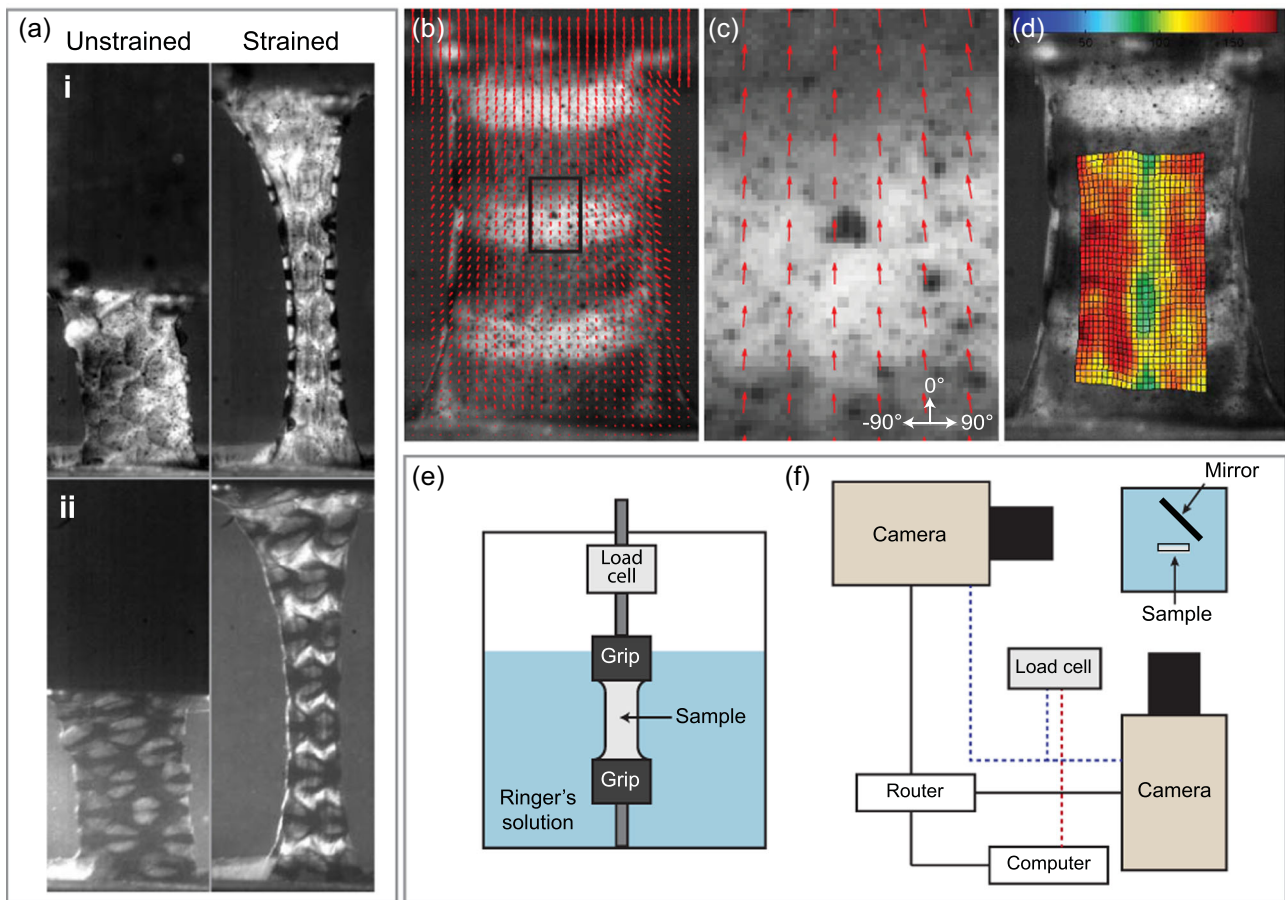
FIGURE 2 Digital image correlation methods and experimental setup. (a) Specimen images from a loading trial with views from the inner surface of the skin (i) and the outer surface of the skin (ii). (b) A specimen image with the displacement vectors shown in red. (c) A zoomed-in version of the midregion (indicated with a black box in b). This image shows the displacement vectors in red, with 0° oriented in the direction of loading. (d) The region of analysis with strain values overlaid; the greatest values are indicated in red and the smallest in blue. (e) Front view of setup, showing the sample in the grips, loaded in the saline water bath (blue). (f) Top view of setup, showing the positions of the high-speed cameras relative to the specimen in the saline bath. The load cell is shown schematically for its connection to the cameras and computer, and was located in line with the specimen, as seen in front view (e).

of specimens during uniaxial testing. A multigrid approach was used in which successively smaller portions of the images were analyzed in greater detail (Eckstein & Vlachos, 2009). In this process, the first pass used a window size of 128 × 128 px with 32 px resolution, where 1 mm is approximately 25 px. The results from this pass were used to predict the displacements of the next iteration, which had a window size of 64 × 64 px with 16 px resolution. The final pass had a window size of 32 × 32 px with a resolution of 8 px. In each pass, the displacement calculations between successive images were predicted by the previous pass and refined to smaller window sizes. Although the images during testing were collected at 50 Hz, correlations were performed at a lower sampling frequency of 5 Hz because analyses at higher frequencies did not reveal additional information. The result of the image correlation for each test yielded the horizontal and vertical components of the displacement field at a resolution of 8 px.

Because the specimen width decreased greatly during testing, we restricted strain calculations to the middle of the specimen, away from the grips, where strains were mostly uniaxial (Figure 2b–d). The

magnitudes and directions of the displacement field were computed at each grid point (Figure 2c) and this analysis was then used to select a 40-px wide region where the strain was mostly uniaxial.

Nominal normal stress was computed by dividing the load by the cross-sectional area of the specimen. For each tensile test, we calculated the following material properties using nominal stress and small-strain assumptions: (1) strength, σ, defined as the maximum stress; 2) extensibility, defined as the small strain at the maximum stress; 3) strain energy, W, or energy to failure, defined as the total area under the stress-strain curve; 4) the modulus of elasticity, E, defined as the slope of the linear region of the stress-strain curve. The assumption of small strain was used for purposes of comparison to previously published values of snake skin (Close & Cundall, 2014; Jayne, 1988; Rivera et al., 2005). For all analyses, only the stress-strain curve before failure was considered. All calculations were conducted using a custom code in MATLAB (Mathworks). Strain energy was calculated using trapezoidal numerical integration of the stress–strain curve, and modulus of elasticity was calculated using a

least-squares linear regression of the linear region of the stress–strain curve (Figure 3).

2.5 | Statistical analyses

We used generalized linear mixed models to analyze mechanical features (extensibility, strength, strain energy, and modulus) because such models allowed us to incorporate intraspecific, interindividual variation as a random effect within the fixed treatment effect (species). We square-root transformed the mechanical data to improve normality in the model residuals. We fitted models using the *lme* function in the R (R Core Team, 2018) package *nlme* (Pinheiro et al., 2014). We first separated our data by orientation (circumferential, longitudinal, and ventral). We then fitted models with the region, species, and their interaction (region × species) as explanatory variables. We treated individual snake ID as a random effect in our models. Residuals from all models were normally distributed.

3 | RESULTS

As shown for representative stress-strain curves (Figure 3), specimens of all species displayed a nonlinear response under uniaxial loading and failed either abruptly or gradually. The failure region was either diagonally or perpendicularly oriented relative to the direction of loading (Figure 4). Ventral specimens of all species generally failed in the gage region (86% of specimens), with tearing always occurring

perpendicular to the loading axis between two scales. Such specimens mostly exhibited abrupt failures (78% of specimens). Circumferential specimens failed in a similar manner, with abrupt failures (71% of specimens) that occurred perpendicular to the loading axis between scales (97% of specimens). Lateral specimens exhibited several failure modes. Some specimens failed abruptly (14% of specimens) and were perpendicular to the loading axis between scales (35% of specimens). Others failed diagonally to the loading axis (56% of specimens) with slower, more progressive failures (86% of specimens). In other cases, failure started near the end of the gage region and ended in the middle (9% of specimens), or vice versa. For
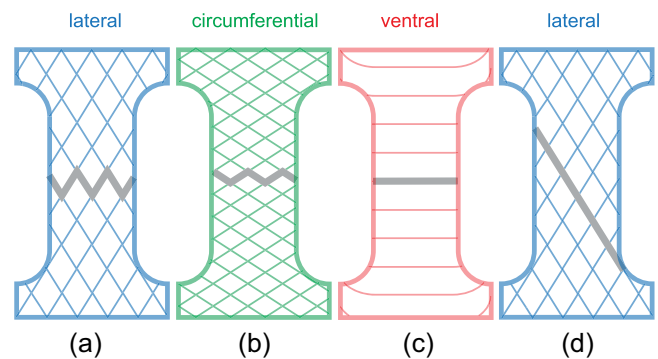

FIGURE 4 Most common failure modes. For all specimens, failure generally occurred in the interscale region, with fracture indicated in gray. (a–c) For most specimens, the pattern of failure was horizontally oriented, orthogonal to the axis of loading. (d) In some lateral specimens, the failure also occurred diagonally to the axis of loading.
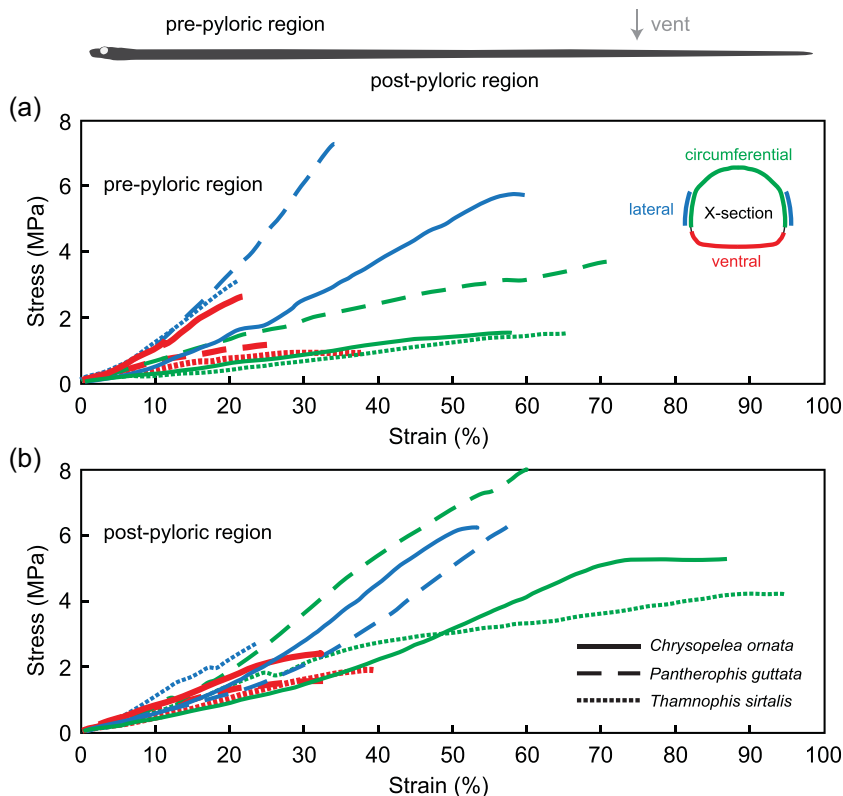

FIGURE 3 Representative stress–strain plots. Samples are shown from each species (*Chrysopelea ornata*, continous line; *Pantherophis guttatus*, dashed line; and *Thamnophis sirtalis*, dotted line) separated by region, pre-pyloric (a) and post-pyloric (b). The location of samples from the body is indicated by color (lateral, blue; circumferential, green; and ventral, red).

all orientations, failure always occurred at a single location within the region of analysis, in particular in the middle of the specimen for most specimens (77% of circumferential, 42% of lateral, and 86% of ventral specimens).

As specimens were loaded, the variation in strain increased nonuniformly throughout the specimen (Figure 5). With increasing displacement, the highest values of strain increased, but regions of low strain persisted (Figure 5a,c). In effect, the range of strain values increased throughout a test, with near-zero strain values remaining. Although the effects of the scalation pattern were not quantified, qualitatively it appeared that scales exhibited some influence on local strain fields. In some specimens, areas of high strain appear to correspond to the regions of skin between the scales, while areas of lower strains correspond to skin directly beneath the scales. Specimens from ventral and circumferential orientations seem to have alternating bands that correspond to these areas. Lateral specimens, however, exhibited less obvious strain patterns, with no clear indication of the effect of scalation.

For circumferential specimens, measurements from pre-pyloric regions resulted in lower estimates of strength compared to post-pyloric regions ($\beta_{\text{pre-pyloric}} = -0.78$, $t = -3.34$, $p = 0.016$), modulus ($\beta_{\text{pre-pyloric}} = -1.28$, $t = -3.33$, $p = 0.016$), extensibility ($\beta_{\text{pre-pyloric}} = -0.13$, $t = -6.54$, $p = 0.001$), and strain energy ($\beta_{\text{pre-pyloric}} = -0.60$, $t = -4.19$, $p = 0.006$) (Tables 3–6; Figure 6). In addition to regional effects, extensibility was also impacted by a species × region interaction, resulting in high post-pyloric and low pre-pyloric extensibility in *C. ornata*, relative to the other species (Table 5; Figure 6a). In longitudinal specimens, strength was lower in the pre-pyloric region ($\beta_{\text{pre-pyloric}} = -0.69$, $t = -2.72$, $p = 0.035$) (Table 4; Figure 6d). We detected no other effects due to region or species for any of the mechanical traits when measurements were taken from lateral or ventral tissue.

4 | DISCUSSION

The main purpose of this study was to provide the first characterization of the material properties of the skin of a flying snake species, *C. ornata*, specifically addressing two functional hypotheses related to gliding locomotion. The first is that the skin of *Chrysopelea* should exhibit greater strength and energy absorption characteristics to deal with the potentially high impact forces of landing. Flying snakes have been observed to land both in the trees and on the ground (personal observations, John J. Socha). The exact kinematics of landing has not been described, but when landing on vegetation, at least one portion of the body must come into contact and absorb the energy of impact (see Socha, 2011, for an example). In a fully developed glide, flying snakes (*C. paradisi*) reach a maximum average velocity of 10 m/s, and they do not slow down before landing. Given this velocity, the change in momentum during landing for a 40 g snake would be 0.4 N·s. Although the impact force cannot be estimated from this energy value without knowing the total contact time of impact, one estimate
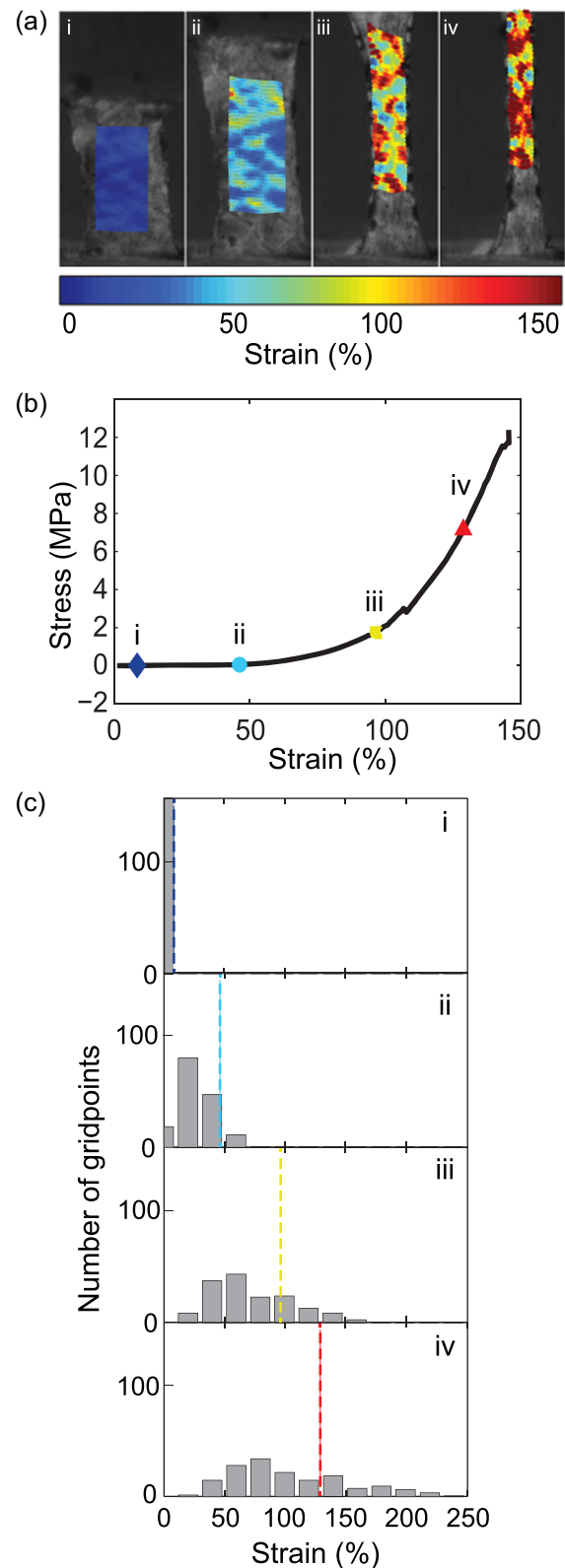

FIGURE 5 Variation in strain through a single stress–strain trial, from a circumferential specimen of *Chrysopelea ornata*. (a) Specimen images shown during the test; i-iv indicate correspondence to average strain values indicated in (b) and (c). (c) Histograms show the distribution of strain over the entire grid region, with the average strain in i-iv indicated with the dashed line.
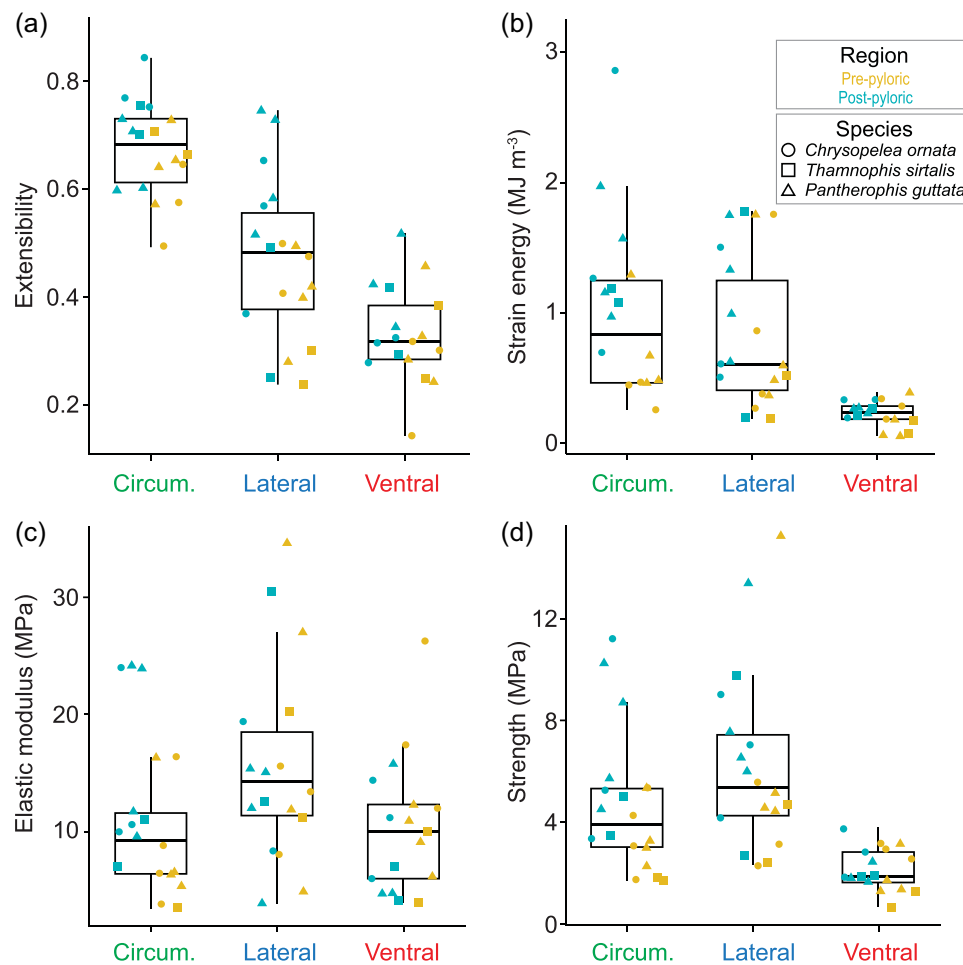
FIGURE 6 Mechanical properties of snake skin specimens for all data analyzed. Summary values of extensibility (a), strain energy (b), elastic modulus (c), and strength (d) are shown in box plots, representing the median and 1first and third quartiles; error bars represent the 95% confidence intervals. Individual specimen data points are shown separated by region (pre-pyloric, yellow; post-pyloric, blue) and species (*Chrysopelea ornata*, circle; *Thamnophis sirtalis*, square; and *Pantherophis guttatus*, triangle). Mean and standard deviations for all data shown are provided in Table 2.

can be made for a rolling landing on the ground: the duration has been estimated to be 50–80 ms (Socha, 2011), providing a maximum impact force of 20X body weight. For a landing on a tree branch or trunk, the contact time may be less, suggesting that the skin would experience even greater forces, particularly if the contact occurs in a localized fashion. More detailed analyses of landing mechanics are required to address this question, and specific measurements of skin displacement during all components of a trajectory, including landing, would help lend insight into the functional role of the skin in flying snakes.

However, our results did not reveal greater strength or energy absorption in the skin of *Chrysopelea* compared to the other species. In fact, the longitudinal specimens from the pre-pyloric region exhibited *lower* strength than *T. sirtalis* and *P. guttatus*. This result suggests that the skin of flying snakes is not specialized for absorbing the impact of landing, though other underlying systems within flying snakes may be. Instead, its skin may be intrinsically sufficient to deal with the impact. It is also possible that the skin exhibits strain-rate-

dependent effects. We chose the extension rate of our testing based on an estimate of movement in the air, but landing strain rates may be much higher than those of aerial undulation.

Second, we hypothesized that the skin of *Chrysopelea* would be more regionally homogenous compared to other species. The rationale for this hypothesis is that when flying snakes become airborne, they flatten the entire body from head to vent, which stretches the skin throughout the body. The skin of *T. sirtalis* exhibits regional differences in extensibility in the circumferential direction, with pre-pyloric skin roughly 50% more extensible and 50% less stiff than post-pyloric skin (Rivera et al., 2005). These differences in *Thamnophis* were attributed to the mechanics of macrophagy feeding, with the anterior body required to accommodate a large food bolus, a challenge with which the posterior body does not have to contend. Our results differ markedly from these previous findings. We found that the circumferential skin of all species exhibited lower extensibility in the pre-pyloric region than in the post-pyloric region; potential differences within these regions were not examined. This

FIGURE 7 Comparisons of average strength with values from a prior study (Jayne, 1988). Lateral and circumferential specimens from the present study are shown with ventrolateral and dorsal specimens from the prior study, respectively. However, these specimens are not analogous (due to differences in orientation and methodology), and the values are shown only for reference.
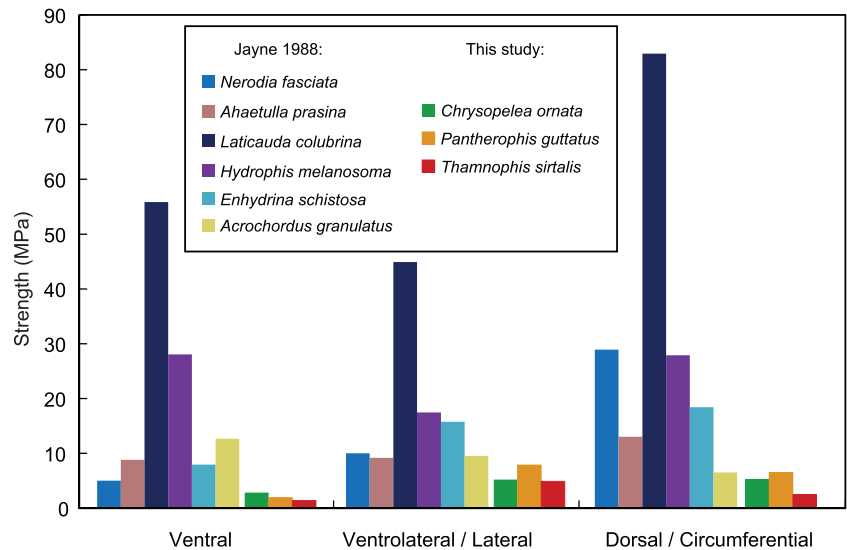
pattern also was found for strength and elastic modulus. One explanation for this reversed pattern is that we used a different method for determining strain. Rivera et al. (2005) determined strain from the extension of the whole sample, calculated using the initial length and the known rate of constant extension. By contrast, we only analyzed the mid-section of the sample and used DIC, which provides localized, higher resolution of a strain field within a sample. As such, our method of determining strain may provide a more accurate representation of the material properties in our reported values, as it excludes effects due to clamping and cross-sectional area changes due to specimen shape.

There have been relatively few prior studies of the material properties of snake skin. In addition to Rivera et al. (2005), our results can also be compared to those of Jayne's pioneering study (Jayne, 1988). As suggested previously, such comparisons should be taken with caution given that different experimental and analytical methods have been used across studies. Our purpose is to provide preliminary comparisons that may help to inform future studies. Here, we compare the strength of our ventral, lateral, and circumferential samples to that of Jayne's ventral, ventrolateral, and dorsal samples, respectively (Figure 7). In this context, the skin of *Chrysopelea* appears even more unremarkable. *Laticauda coubrina*, *Hydrophis melansoma*, and *Enhydrina schistosa*, sea snakes from the family Elapidae, all show much greater strength across all sample types than *Chrysopelea*. *Ahaetulla prasina* also showed greater strength; as a close relative of *Chrysopelea* (a member of the sub-family Ahaetuliinae), this comparison provides more preliminary evidence that the skin of *Chrysopelea* is not functionally specialized for gliding locomotion.

4.1 | Study limitations

In addition to lacking an explicitly phylogenetic approach, this study was constrained by sampling. Although we conducted testing on a relatively large number of samples, the number of individuals per species was small, limiting the power of statistical comparisons. Testing the full range of five

species within the genus *Chrysopelea* would also be informative. The single flying snake species tested here, *C. ornata*, does not glide as well as *C. paradisi* (Socha & LaBarbera, 2005). Both cross-sectional shape (Holden et al., 2014; Krishnan et al., 2014) and relative body posture are important for the generation of aerodynamic forces, and undulatory patterns additionally influence the snake's stability characteristics (Jafari et al., 2014, 2017; Yeaton et al., 2020). It is possible that skin-property-related features may influence differences in flattening ability and ability to produce specific kinematics in the air, and thus the locomotor performance of the snake during gliding.

Future studies might also explore trends in our data, where lack of statistical significance might have resulted from small sample sizes; large effect sizes without significance suggests that low power might have driven the results. Although not statistically significant, it appeared that extensibility is higher in circumferential samples compared to longitudinal or ventral ones, across species. This result is consistent with other studies conducted on tissues having an in vivo tubular structure (McGuire, Abramowitch, et al., 2019; McGuire, Crandall, et al., 2019), where the circumferential stresses are generally higher than the axial stresses. Additionally, the ventral samples appeared to exhibit lower and less variable strain energy and strength than longitudinal or circumferential samples. Such studies may also benefit from biaxial rather than uniaxial testing (Skulborstad et al., 2015), because biaxial testing may more accurately recreate the loading that occurs in vivo and capture the anisotropy of the snake's skin. The snake's skin should deform much less under equi-biaxial loading compared to uniaxial loading at an equal load magnitude. This is because, during biaxial testing, all edges of square specimens are usually constrained and loaded simultaneously, whereas in uniaxial tests the longer edges of rectangular specimens are not constrained and loaded, resulting in greater deformation in the direction of loading. However, we expect that some differences in strains in the longitudinal and circumferential directions would still be detected during biaxial testing, although to a lesser extent because the microstructural components of the

TABLE 1 Test specimen numbers

	Chrysopelea ornata		*Pantherophis guttatus*		*Thamnophis sirtalis*	
	Pre-pyloric	Post-pyloric	Pre-pyloric	Post-pyloric	Pre-pyloric	Post-pyloric
Lateral	15	7	16	20	6	2
Circumferential	14	6	21	16	5	2
Ventral	14	8	10	11	3	3

TABLE 2 Material properties of *Chrysopelea ornata*, *Pantherophis guttatus*, and *Thamnophis sirtalis*

	Lateral		Circumferential		Ventral	
	Pre	Post	Pre	Post	Pre	Post
Chrysopelea ornata						
Ultimate strength (MPa)	3.37	6.75	3.03	6.61	2.89	2.80
	(1.40)	(3.44)	(1.10)	(4.07)	(1.06)	(0.89)
Strain energy (MJ·m^{-3})	0.51	0.80	0.39	1.61	0.27	0.29
	(0.29)	(0.63)	(0.14)	(1.36)	(0.19)	(0.10)
Extensibility	0.56	0.53	0.57	0.79	0.26	0.31
	(0.12)	(0.15)	(0.10)	(0.18)	(0.22)	(0.05)
Elastic modulus (MPa)	12.38	14.59	6.40	14.86	18.59	10.56
	(6.53)	(9.25)	(2.60)	(13.00)	(12.22)	(4.83)
Pantherophis guttatus						
Ultimate strength (MPa)	7.37	8.38	3.48	7.32	1.88	1.98
	(5.48)	(3.83)	(1.67)	(3.81)	(1.02)	(0.66)
Strain energy (MJ·m^{-3})	0.80	1.18	0.73	1.42	0.18	0.26
	(0.67)	(0.63)	(0.38)	(0.83)	(0.14)	(0.13)
Extensibility	0.40	0.64	0.65	0.66	0.33	0.43
	(0.14)	(0.17)	(0.14)	(0.13)	(0.12)	(0.11)
Elastic modulus (MPa)	19.66	11.64	8.71	17.39	9.68	8.46
	(12.04)	(12.32)	(4.58)	(11.90)	(4.32)	(1.94)
Thamnophis sirtalis						
Ultimate strength (MPa)	3.55	6.22	1.77	4.25	0.96	1.88
	(2.40)	(4.99)	(0.63)	(1.14)	(0.51)	(0.48)
Strain energy (MJ·m^{-3})	0.36	0.99	0.39	1.14	0.13	0.24
	(0.31)	(1.12)	(0.32)	(0.50)	(0.09)	(0.12)
Extensibility	0.27	0.37	0.68	0.73	0.32	0.36
	(0.09)	(0.17)	(0.20)	(0.16)	(0.08)	(0.13)
Elastic modulus (MPa)	15.73	21.58	3.54	9.09	7.01	5.59
	(7.92)	(12.64)	(0.94)	(2.34)	(1.42)	(2.19)

Note: Peak values of stress, strain energy, and extensibility are reported, and elastic modulus is calculated in the linear region of the stress–strain curve. Values shown reflect the average across samples for the condition shown, with the standard deviation provided in parentheses.

snake skin (such as collagen fibers) have less freedom to reorganize themselves during biaxial loading. The effects of such microstructural rearrangement during loading should be quantified to better characterize the mechanics of the snake skin by combining the DIC method with other optical techniques such as optical coherence tomography (Donaldson et al., 2022).

Lastly, we used an assumption of small strain to characterize the deformations of our specimens, but clearly, the specimens

JEZ-A ECOLOGICAL AND INTEGRATIVE PHYSIOLOGY —WILEY—

TABLE 3 Analysis of strength for the three snake species included in this study

	β Coefficient	Standard error	t Value	Two-sided p value
(A) *Circumferential measurements*				
Intercept	**2.49**	0.27	9.21	0.001
Region (pre-pyloric)	**−0.78**	0.23	−3.34	0.016
Species (*Pantherophis guttatus*)	0.18	0.36	0.50	0.632
Species (*Thamnophis sirtalis*)	−0.44	0.43	−1.02	0.345
Region (pre-pyloric) × species (*P. guttatus*)	−0.05	0.31	−0.17	0.874
Region (pre-pyloric) + species (*T. sirtalis*)	0.05	0.37	0.15	0.889
(B) *Longitudinal measurements*				
Intercept	**2.57**	0.38	6.68	0.001
Region (pre-pyloric)	**−0.69**	0.25	−2.72	0.035
Species (*P. guttatus*)	0.29	0.51	0.57	0.591
Species (*T. sirtalis*)	−0.19	0.61	−0.31	0.770
Region (pre-pyloric) × species (*P. guttatus*)	0.44	0.33	1.31	0.237
Region (pre-pyloric) + species (*T. sirtalis*)	0.17	0.40	1.31	0.692
(C) *Ventral measurements*				
Intercept	**1.66**	0.13	12.92	<0.001
Region (pre-pyloric)	0.04	0.12	0.35	0.744
Species (*P. guttatus*)[a]	−0.29	0.18	−1.61	0.158
Species (*T. sirtalis*)	−0.29	0.20	−1.41	0.209
Region (pre-pyloric) × species (*P. guttatus*)[a]	−0.06	0.17	−0.37	0.724
Region (pre-pyloric) + species (*T. sirtalis*)[a]	−0.44	0.19	−2.32	0.068

Note: Mixed model output is shown for (A) circumferential measurements, (B) longitudinal measurements, and (C) ventral measurements. Significant ($p < 0.05$) coefficients are shown in bold. Unless otherwise indicated, degrees of freedom = 6 in all models.
[a]Degrees of freedom = 5.

TABLE 4 Analysis of modulus for the three snake species included in this study

	β Coefficient	Standard error	t Value	Two-sided p value
(A) *Circumferential measurements*				
Intercept	**3.77**	0.45	8.40	<0.001
Region (pre-pyloric)	**−1.28**	0.38	−3.33	0.016
Species (*Pantherophis guttatus*)	0.32	0.59	0.53	0.615
Species (*Thamnophis sirtalis*)	−0.78	0.71	−1.09	0.316
Region (pre-pyloric) × species (*P. guttatus*)	0.06	0.51	0.12	0.910
Region (pre-pyloric) + species (*T. sirtalis*)	0.16	0.61	0.27	0.797
(B) *Longitudinal measurements*				
Intercept	**3.76**	0.65	5.77	0.001
Region (pre-pyloric)	−0.27	0.92	−0.30	0.776
Species (*P. guttatus*)	−0.44	0.86	−0.51	0.626
Species (*T. sirtalis*)	0.78	1.03	0.76	0.478
Region (pre-pyloric) × species (*P. guttatus*)	1.15	1.22	0.94	0.382
Region (pre-pyloric) + species (*T. sirtalis*)	−0.34	1.46	−0.24	0.822

(Continues)

TABLE 4 (Continued)

	β Coefficient	Standard error	t Value	Two-sided p value
(C) *Ventral measurements*				
Intercept	**3.20**	0.42	7.58	<0.001
Region (pre-pyloric)	1.06	0.49	2.14	0.086
Species (*P. guttatus*)[a]	−0.39	0.59	−0.66	0.531
Species (*T. sirtalis*)	−0.86	0.67	−1.28	0.247
Region (pre-pyloric) × species (*P. guttatus*)[a]	−0.78	0.68	−1.13	0.308
Region (pre-pyloric) + species (*T. sirtalis*)[a]	−0.82	0.78	−1.04	0.343

Note: Mixed model output is shown for (A) circumferential measurements, (B) longitudinal measurements, and (C) ventral measurements. Significant ($p < 0.05$) coefficients are shown in bold. Unless otherwise indicated, degrees of freedom = 6 in all models.
[a]Degrees of freedom = 5.

TABLE 5 Analysis of extensibility for the three snake species included in this study

	β Coefficient	Standard error	t Value	Two-sided p value
(A) *Circumferential measurements*				
Intercept	**0.89**	0.02	40.24	<0.001
Region (pre-pyloric)	**−0.13**	0.02	−6.54	0.001
Species (*Pantherophis guttatus*)	**−0.08**	0.03	−2.60	0.041
Species (*Thamnophis sirtalis*)	−0.03	0.03	−0.99	0.359
Region (pre-pyloric) × species (*P. guttatus*)	**0.13**	0.03	4.71	0.003
Region (pre-pyloric) + species (*T. sirtalis*)	**0.11**	0.03	3.36	0.015
(B) *Longitudinal measurements*				
Intercept	**0.72**	0.05	15.69	<0.001
Region (pre-pyloric)	−0.05	0.06	−0.74	0.489
Species (*P. guttatus*)	0.08	0.06	1.25	0.257
Species (*T. sirtalis*)	−0.12	0.07	−1.69	0.143
Region (pre-pyloric) × species (*P. guttatus*)	−0.13	0.08	−1.55	0.171
Region (pre-pyloric) + species (*T. sirtalis*)	−0.04	0.10	−0.37	0.723
(C) *Ventral measurements*				
Intercept	**0.55**	0.04	12.77	<0.001
Region (pre-pyloric)	−0.06	0.06	−0.91	0.406
Species (*P. guttatus*)[a]	0.10	0.06	1.63	0.155
Species (*T. sirtalis*)	0.04	0.07	0.59	0.578
Region (pre-pyloric) × species (*P. guttatus*)[a]	−0.03	0.08	−0.33	0.754
Region (pre-pyloric) + species (*T. sirtalis*)[a]	0.02	0.10	0.22	0.832

Note: Mixed model output is shown for (A) circumferential measurements, (B) longitudinal measurements, and (C) ventral measurements. Significant ($p < 0.05$) coefficients are shown in bold. Unless otherwise indicated, degrees of freedom = 6 in all models.
[a]Degrees of freedom = 5.

experienced large strains during uniaxial testing. This method of calculation was done primarily to compare our findings with those of previously published studies (Close & Cundall, 2014; Jayne, 1988; Rivera et al., 2005), where small strains were simply measured from the clamp displacement of uniaxial tensile machines. For this reason, our reported DIC-based calculated strains underestimate the actual strains that the snake's skin experienced ex vivo under uniaxial loading. Together with a larger

TABLE 6 Analysis of strain energy for the three snake species included in this study

	β Coefficient	Standard error	t Value	Two-sided p value
(A) *Circumferential measurements*				
Intercept	**1.22**	0.13	9.10	<0.001
Region (pre-pyloric)	**−0.60**	0.14	−4.19	0.006
Species (*Pantherophis guttatus*)	−0.04	0.18	−0.21	0.843
Species (*Thamnophis sirtalis*)	−0.15	0.21	−0.72	0.498
Region (pre-pyloric) × species (*P. guttatus*)	0.25	0.19	1.34	0.230
Region (pre-pyloric) + species (*T. sirtalis*)	0.16	0.23	0.70	0.513
(B) *Longitudinal measurements*				
Intercept	**0.91**	0.18	5.08	0.002
Region (pre-pyloric)	−0.22	0.14	−1.52	0.179
Species (*P. guttatus*)	0.16	0.24	0.68	0.523
Species (*T. sirtalis*)	−0.02	0.28	−0.06	0.955
Region (pre-pyloric) × species (*P. guttatus*)	0.00	0.19	0.01	0.990
Region (pre-pyloric) + species (*T. sirtalis*)	−0.09	0.23	−0.41	0.693
(C) *Ventral measurements*				
Intercept	0.53	0.06	8.28	<0.001
Region (pre-pyloric)	−0.02	0.09	−0.18	0.867
Species (*P. guttatus*)[a]	−0.03	0.09	−0.31	0.766
Species (*T. sirtalis*)	−0.05	0.10	−0.46	0.665
Region (pre-pyloric) × species (*P. guttatus*)[a]	−0.10	0.12	−0.84	0.439
Region (pre-pyloric) + species (*T. sirtalis*)[a]	−0.12	0.14	−0.89	0.414

Note: Mixed model output is shown for (A) circumferential measurements, (B) longitudinal measurements, and (C) ventral measurements. Significant ($p < 0.05$) coefficients are shown in bold. Unless otherwise indicated, degrees of freedom = 6 in all models.

[a]Degrees of freedom = 5.

number of specimens and biaxial testing methods, future mechanical analysis of the snake's skin should be based on the measurements of deformations using finite strain theory (rather than infinitesimal strain theory).

5 | CONCLUSIONS

Our investigation of the material properties in *C. ornata*, *T. sirtalis*, and *P. guttatus* suggests that the skin of flying snakes (*Chrysopelea*) is not specialized for gliding locomotion. Nonetheless, it is striking how similar the mechanical properties of skin are among all three snake species, which are phylogenetically and ecologically divergent from each other. When interpreted in an evolutionary context, our results suggest that the mechanical properties of *Chrysopelea* snake skin are preadapted for gliding flight and substrate collision. If so, then the origin of gliding is likely more limited by the evolution of a highly specialized behavioral repertoire (Socha, 2011) than by morphological specializations. When compared to other colubrids, gliding snakes

do not occupy a distinct portion of morphospace, suggesting that specialization in the skin or skeletal anatomy is not a prerequisite for specialized gliding to evolve. Alternatively, it is plausible that the kinematics of gliding and impact, while visually quite striking, are not as mechanically demanding as previously thought. As the field of biomechanics expands to include more species and more open-source data (Muñoz & Price, 2019), addressing the mechanisms of biomechanical diversity will become increasingly within our reach.

CONFLICT OF INTEREST

The authors declare no conflict of interest.

ORCID

John J. Socha http://orcid.org/0000-0002-4465-1097

REFERENCES

Alibardi, L. (2005). Differentiation of snake epidermis, with emphasis on the shedding layer. *Journal of Morphology*, 264(2), 178–190.

Chan, R. W., & Titze, I. R. (2003). Effect of postmortem changes and freezing on the viscoelastic properties of vocal fold tissues. *Annals of Biomedical Engineering*, 31(4), 482–491.

Cinelli, A. R., Wang, D., Chen, P., Liu, W., & Halpern, M. (2002). Calcium transients in the garter snake vomeronasal organ. *Journal of Neurophysiology*, 87(3), 1449–1472.

Clavert, P., Kempf, J. F., Bonnomet, F., Boutemy, P., Marcelin, L., & Kahn, J. L. (2001). Effects of freezing/thawing on the biomechanical properties of human tendons. *Surgical and Radiologic Anatomy*, 23(4), 259–262.

Close, M., & Cundall, D. (2014). Snake lower jaw skin: Extension and recovery of a hyperextensible keratinized integument. *Journal of Experimental Zoology Part A: Ecological Genetics and Physiology*, 321(2), 78–97.

Donaldson, K., Thomas, J., Zhu, Y., Clark-Deener, S., Alperin, M., & De Vita, R. (2022). In-plane and out-of-plane deformations of gilt utero-sacral ligaments. *Journal of the Mechanical Behavior of Biomedical Materials*, 131, 105249.

Eckstein, A., & Vlachos, P. P. (2009). Digital particle image velocimetry (DPIV) robust phase correlation. *Measurement Science and Technology*, 20(5), 055401.

Figueroa, A., McKelvy, A. D., Grismer, L. L., Bell, C. D., & Lailvaux, S. P. (2016). A species-level phylogeny of extant snakes with description of a new colubrid subfamily and genus. *PLoS One*, 11(9), e0161070.

Foutz, T. L., Stone, E. A., & Abrams, C.F., Jr. (1992). Effects of freezing on mechanical properties of rat skin. *American Journal of Veterinary Research*, 53(5), 788–792.

Frolich, L. M. (1997). The role of the skin in the origin of amniotes: Permeability barrier, protective covering and mechanical support. In S. S. Sumida, & K. L. M. Martin. (Eds.), *Amniote origins*. Academic Press.

Gans, C. (1953). The functional morphology of the egg-eating adaptations in the snake genus *Dasypeltis*. *Zoologica New York*, 37, 209–244.

Holden, D., Socha, J. J., Cardwell, N. D., & Vlachos, P. P. (2014). Aerodynamics of the flying snake *Chrysopelea paradisi*: How a bluff body cross-sectional shape contributes to gliding performance. *Journal of Experimental Biology*, 217(3), 382–394.

Hu, D. L., Nirody, J., Scott, T., & Shelley, M. J. (2009). The mechanics of slithering locomotion. *Proceedings of the National Academy of Sciences of the United States of America*, 106(25), 10081–10085.

Jackson, D. W., Grood, E. S., Cohn, B. T., Arnoczky, S. P., Simon, T. M., & Cummings, J. F. (1991). The effects of in situ freezing on the anterior cruciate ligament. *The Journal of Bone & Joint Surgery*, 73(2), 201–213.

Jackson, M. K., & Reno, H. W. (1975). Comparative skin structure of some fossorial and subfossorial leptotyphlopid and colubrid snakes. *Herpetologica*, 31(3), 350–359.

Jafari, F., Ross, S. D., Vlachos, P. P., & Socha, J. J. (2014). A theoretical analysis of pitch stability during gliding in flying snakes. *Bioinspiration & Biomimetics*, 9(2), 025014.

Jafari, F., Tahmasian, S., Ross, S. D., & Socha, J. J. (2017). Control of gliding in a flying snake-inspired n-chain model. *Bioinspiration & Biomimetics*, 12(6), 066002.

Jayne, B. C. (1988). Mechanical behaviour of snake skin. *Journal of Zoology*, 214, 125–140.

Jørgensen, P. H., Andreassen, T. T., & Jørgensen, K. D. (1989). Growth hormone influences collagen deposition and mechanical strength of intact rat skin. A dose-response study. *Acta Endocrinologica*, 120(6), 767–772. https://doi.org/10.1530/acta.0.1200767

Krishnan, A., Socha, J. J., Vlachos, P. P., & Barba, L. A. (2014). Lift and wakes of flying snakes. *Physics of Fluids*, 26(3), 031901.

Licht, P., & Bennett, A. F. (1972). A scaleless snake: Tests of the role of reptilian scales in water loss and heat transfer. *Copeia*, 1972(4), 702–707.

Lillywhite, H. B. (1993). Subcutaneous compliance and gravitational adaptation in snakes. *Journal of Experimental Zoology*, 267(6), 557–562.

Marangoni, R. D., Glaser, A. A., Must, J. S., Brody, G. S., Beckwith, T. G., Walker, G. R., & White, W. L. (1966). Effect of storage and handling techniques on skin tissue properties. *Annals of the New York Academy of Sciences*, 136(16), 441–453.

McGuire, J. A., Abramowitch, S. D., Maiti, S., & De Vita, R. (2019). Swine vagina under planar biaxial loads: An investigation of large deformations and tears. *Journal of Biomechanical Engineering*, 141(4), 041003.

McGuire, J. A., Crandall, C. L., Abramowitch, S. D., & De Vita, R. (2019). Inflation and rupture of vaginal tissue. *Interface Focus*, 9(4), 20190029.

Moon, B. R. (2000). The mechanics of swallowing and the muscular control of diverse behaviours in gopher snakes. *Journal of Experimental Biology*, 203(17), 2589–2601.

Muñoz, M. M., & Price, S. A. (2019). The future is bright for evolutionary morphology and biomechanics in the era of big data. *Integrative and Comparative Biology*, 59(3), 599–603.

Osorio, D., & Srinivasan, M. V. (1991). Camouflage by edge enhancement in animal coloration patterns and its implications for visual mechanisms. *Proceedings of the Royal Society B*, 244(1310), 81–85.

Pyron, R., Burbrink, F. T., & Wiens, J. J. (2013). A phylogeny and revised classification of Squamata, including 4161 species of lizards and snakes. *BMC Evolutionary Biology*, 13(93), 93.

Quirinia, A., & Viidik, A. (1991). Freezing for postmortal storage influences the biomechanical properties of linear skin wounds. *Journal of Biomechanics*, 24(9), 819–823.

Rivera, G., Savitzky, A. H., & Hinkley, J. A. (2005). Mechanical properties of the integument of the common gartersnake, *Thamnophis sirtalis* (Serpentes: Colubridae). *Journal of Experimental Biology*, 208(15), 2913–2922.

R Core Team (2018) *R: A language and environment for statistical computing*. R Foundation for Statistical Computing. https://www.r-project.org/

Pinheiro, J., Bates, D., DebRoy, S., & D. Sarkar (2014) *nlme: Linear and nonlinear mixed effects models*. R package version 3.1. http://cran.r-project.org/web/packages/nlme.index.html

Savitzky, A. H., Townsend, V. R., Hutchinson, Jr., D. A., & Mori, A. (2004). Dermal characteristics, scale row organization, and the origin of macrostomy in snakes. *Journal of Morphology*, 260, 325.

Skulborstad, A. J., Swartz, S. M., & Goulbourne, N. C. (2015). Biaxial mechanical characterization of bat wing skin. *Bioinspiration & Biomimetics*, 10(3), 036004.

Socha, J. J. (2002). Gliding flight in the paradise tree snake. *Nature*, *418*, 603–604.

Socha, J. J. (2006). Becoming airborne without legs: The kinematics of take-off in a flying snake, *Chrysopelea paradisi*. *Journal of Experimental Biology*, *209*(17), 3358–3369.

Socha, J. J. (2011). Gliding flight in *Chrysopelea*: Turning a snake into a wing. *Integrative and Comparative Biology*, *51*(6), 969–982.

Socha, J. J., & LaBarbera, M. (2005). Effects of size and behavior on aerial performance of two species of flying snakes (*Chrysopelea*). *Journal of Experimental Biology*, *208*(10), 1835–1847.

Socha, J. J., Miklasz, K., Jafari, F., & Vlachos, P. P. (2010). Non-equilibrium trajectory dynamics and the kinematics of gliding in a flying snake. *Bioinspiration & Biomimetics*, *5*(4), 045002.

Woo, S. L. Y., Orlando, C. A., Camp, J. F., & Akeson, W. H. (1986). Effects of postmortem storage by freezing on ligament tensile behavior. *Journal of Biomechanics*, *19*(5), 399–404.

Wu, J. Z., Cutlip, R. G., Andrew, M. E., & Dong, R. G. (2007). Simultaneous determination of the nonlinear-elastic properties of skin and subcutaneous tissue in unconfined compression tests. *Skin Research and Technology*, *13*(1), 34–42.

Yeaton, I. J., Ross, S. D., Baumgardner, G. A., & Socha, J. J. (2020). Undulation enables gliding in flying snakes. *Nature Physics*, *16*(9), 974–982.

Zhang, J., Jin, G. C., Meng, L. B., Jian, L. H., Wang, A. Y., & Lu, S. B. (2005). Strain and mechanical behavior measurements of soft tissues with digital speckle method. *Journal of Biomedical Optics*, *10*(3), 034021.

SUPPORTING INFORMATION

Additional supporting information can be found online in the Supporting Information section at the end of this article.